

EVIDENCE FOR CONVECTION IN SUNSPOT PENUMBRAE

L. BHARTI¹, S. K. SOLANKI^{1,2} AND J. HIRZBERGER¹1. Max-Planck-Institute für Sonnensystemforschung, Max-Planck-Str. 2, 37191 Katlenburg-Lindau, Germany and
2. School of Space Research, Kyung Hee University, Yongin, Gyeonggi Do, 446-701, Korea

Received; Accepted

ABSTRACT

We present an analysis of twisting motions in penumbral filaments in sunspots located at heliocentric angles from 30° to 48° using three time series of blue continuum images obtained by the Broadband Filter Imager (BFI) onboard *Hinode*. The relations of the twisting motions to the filament brightness and the position within the filament and within the penumbra, respectively, are investigated. Only certain portions of the filaments show twisting motions. In a statistical sense, the part of the twisting portion of a filament located closest to the umbra is brightest and possesses the fastest twisting motion, with a mean twisting velocity of 2.1 km s^{-1} . The middle and outer sections of the twisting portion of the filament (lying increasingly further from the umbra), which are less bright, have mean velocities of 1.7 km s^{-1} and 1.35 km s^{-1} , respectively. The observed reduction of brightness and twisting velocity towards the outer section of the filaments may be due to reducing upflow along the filament's long axis. No significant variation of twisting velocity as a function of viewing angles was found. The obtained correlation of brightness and velocity suggests that overturning convection causes the twisting motions observed in penumbral filament and may be the source of the energy needed to maintain the brightness of the filaments.

Subject headings: Sun: convection – sunspots – Sun: granulation

1. INTRODUCTION

A central question related to sunspots is how sufficient energy can be transported through a strong magnetic field, that reaches well below the solar surface (a deep penumbra, Solanki & Schmidt 1993), to keep the penumbra as bright as it is. It is generally assumed that some form of magnetoconvection exists in penumbrae, acting in conjunction with the complex structuring of the magnetic and flow fields (see Solanki 2003 and Scharmer 2009 for reviews). Recently, 3D radiative MHD simulations have provided support for this conjecture (Heinemann et al. 2007; Rempel et al. 2009a; 2009b). Observational support has been less clear-cut, however.

The twisting motion of penumbral filaments observed by Ichimoto et al. (2007) opens a new window to understanding the nature of penumbral filaments and potentially of small-scale magnetoconvection and penumbral energy transport. In sunspots located away from disk center, filaments oriented roughly perpendicular to the disk radius vector display a twisting motion that is always directed from the limb-side to the center-side of the filament. As deduced by Zakharov et al. (2008), these twisting motions are a manifestation of overturning convection, associated with bright filaments. According to Spruit et al. (2010) the dark stripes follow the direction of inclined magnetic field lines. In the present article we investigate these twisting motions in a large ensemble of filaments and in different parts of filaments, allowing us to statistically determine their properties and the relationship with other parameters of the filaments. In particular, we are interested in determining whether the heat transport from below associated with these motions contributes to the observed brightness of the penumbra.

2. OBSERVATIONS

For the present study we selected time series of blue continuum (4500 \AA) images of sunspots located away from disk center observed with the Broadband Filter Imager (BFI) of the Solar Optical Telescope (SOT) onboard *Hinode* (Tsuneta et al. 2007). The first time series, recorded on January 9, 2007, consists of 498 images at 30 s cadence and contains a sunspot (NOAA 10933) located at a heliocentric angle of $\theta = 48^\circ$. The other two time series, covering another sunspot (NOAA 10923), were recorded on November 11 and 12, 2006, at heliocentric angles of $\theta = 38^\circ$ and $\theta = 30^\circ$, respectively. They contain 292 and 191 images, respectively, at a cadence of 20 s. The spatial resolution in the blue continuum is $0''.2$. The image scale is $0''.054$ per pixel. Raw data were corrected for flat field and dark current using the SolarSoft pipelines for the *Hinode* SOT/BFI. A Wiener filter (Sobotka et al. 1993) was applied to all images to correct the point spread function of the telescope assuming diffraction on an ideal circular 50 cm aperture. Finally, contributions of five-minute oscillations were filtered by means of a subsonic filter (Title et al. 1989) with a cut-off velocity of 6 km s^{-1} . The first and last 15 images from time series of January 9, 2007 and similarly 10 images from November 11 and 12, 2006 have been omitted due to the apodizing window used in the subsonic filtering. Intensities in all images are normalized to the mean intensity of quiet regions close to the observed sunspot. Time series of these observations have been presented by Ichimoto et al. (2007).

3. ANALYSIS

Figure 1 shows a blue continuum image as obtained on January 9, 2007. The sunspot is located at $\theta = 48^\circ$. An animation of the time series of such blue continuum images reveals a lateral motion of dark lanes in the

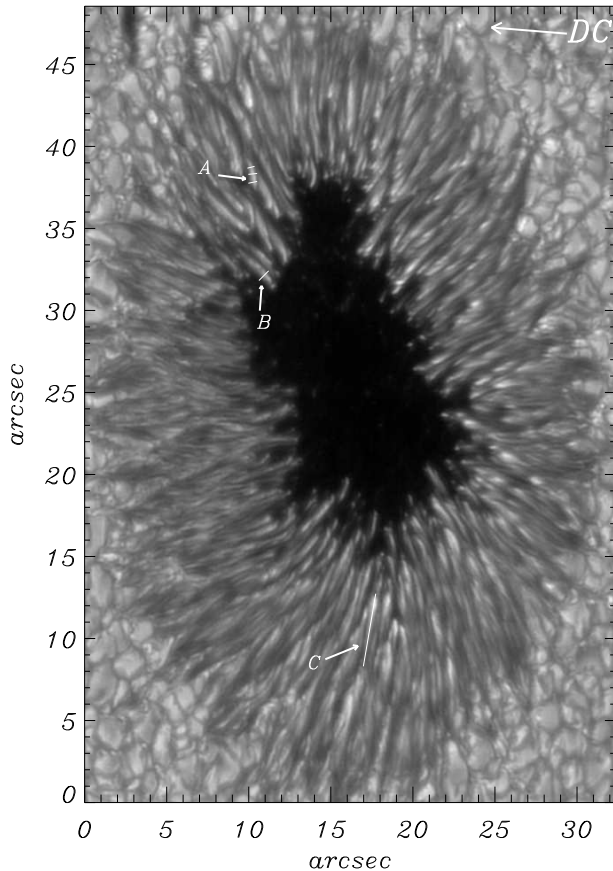


FIG. 1.— A sunspot image in the blue continuum taken on January 9, 2007 by the SOT/BFI aboard Hinode. The direction to disk center is shown by the arrow indicating 'DC' at the upper right corner. 'A' points to the location of time slices at the inner cut, middle cut and outer cut (from below) of a penumbral filament (see the main text and Fig. 2 for definitions). Location of time slices for another penumbral filaments is marked by 'B'. The location of the intensity profile along filament 'C' is marked by a white line.

filaments from the limb-side to the disk-center-side in penumbral sections where the filaments are oriented at angles smaller than $\pm 60^\circ$ to the nearest part of the solar limb. We have studied such motions in relation to other properties of 21 filaments in the northern section and 22 in the southern section. We note that such twists are discernable only within a certain portion of the length of a filament. We divided each filament into 3 parts (cf. Fig. 2), a central part displaying a twist (henceforth called the body of the filament) and two parts bounding this central part that do not display any discernable twisting motions. These include the 'head' of a filament i.e. the bright innermost part of the filament, and the 'tail' of a filament, the often faint outer part in which no twist is seen anymore in space-time diagrams. Here, 'inner' and 'outer' parts of filaments refer to the parts closer to the inner and to the outer boundary of the penumbra, respectively. The locations of the boundaries between head, body and tail vary from filament to filament. E.g., we find that filaments which extend into the umbra, possess twist over their whole length, although in the darker outer (i.e. away from umbra) part of the filament it becomes difficult to identify such a twisting motion. We call the length of the twisting portion (body) of the filament its twisting length.

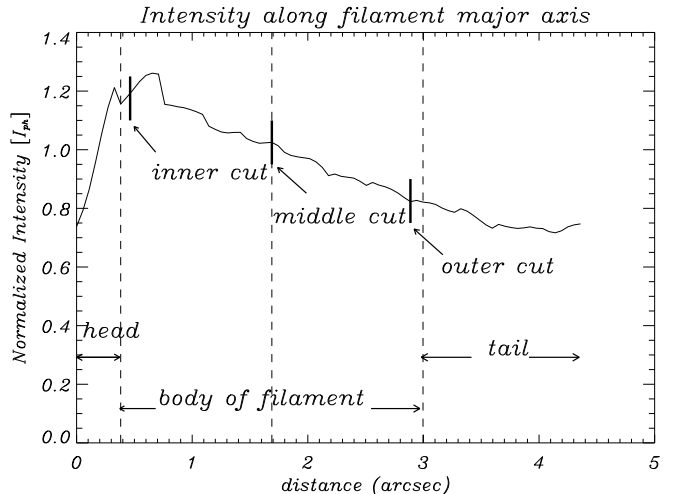


FIG. 2.— Normalized intensity profile along the major axis of a typical penumbral filament. The plotted profile corresponds to the filament marked 'C' in Fig. 1. The intensity decreases from the bright head towards the outer section (i.e. with distance from umbra). Various terms defined in the main text are illustrated.

The 'twisting length' defined above may not be constant over the time series for each filament. The twisting length of filaments discussed later (Fig. 4 (right)) refers to the beginning of the time series. The twisting length of filaments which extend into the umbra, displays some ambiguity.

We made space time diagrams for three locations in the body of the filament. These three locations are the 'inner cut' which is close to the inner edge of the body of the filament, the 'middle cut' is the middle point of the body of the filament and the 'outer cut' which is 2-3 pixels inside the outer edge of the body of the filament, such that dark stripes can still be seen in the space-time diagram. The locations of all these parts are sketched for filament 'C' in Fig. 2. The location of this particular filament 'C' is marked in Figure 1. Note that the absence of a clear signal does not imply the absence of corresponding motions in the head or tail of a filament, just the absence of dark stripes parallel to the filament's axis that make such motions visible.

The width of a (twisting) filament is the distance between the inflection points of the intensity profiles parallel to the filament's minor axis.

From Fig. 1 one can see that the inner part of a typical penumbral filament is brighter and the brightness decreases gradually towards the outer part. This is generally true, irrespective of whether the filament is located in the inner, middle or outer penumbra. The intensity profile along a filament's major axis as plotted in Fig. 2, is thus relatively typical of many filaments.

Space-time diagrams of various locations, marked by arrows and white lines in Fig. 1, in some of the studied filaments are shown in Fig. 3. The motion of thin dark stripes across the filaments is apparent as inclined dark stripes in Figs. 3, producing the impression of twisting filaments, or, more precisely, of horizontal motions perpendicular to the filament's major axes from the limb-side to the center-side. We stress that in our data set these motions are manifested only by brightness varia-

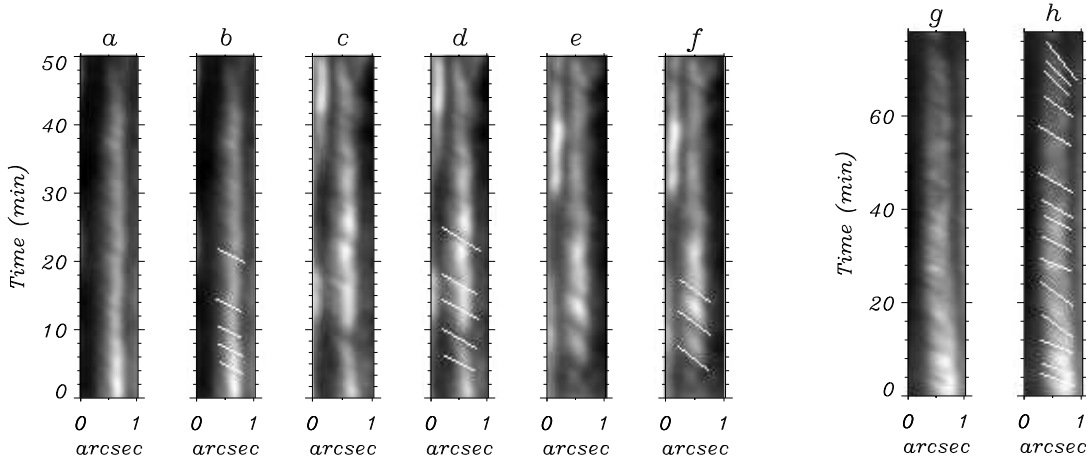


FIG. 3.— Space-time slices (a to f) at the three locations marked by 'A' in Fig. 1. Panels a and b refer to the inner cut, c and d to the middle cut and e, f to the outer cut of filament 'A' (see Fig. 2 and the main text for a definition of these terms). Panels b, d and f are the same as a, c and e, but with lines overlying the dark stripes to better reveal their slopes, which are indicative of proper motion velocity. Panel g and h are space-time slices for filament 'B' at a fixed slice position. Panel h repeats panel g, but with white lines overplotting the dark stripes.

tions and need not necessarily correspond to a physical twist of the filaments. The slopes of these stripes are proportional to the velocities of the horizontal motions of dark structures in the filaments. The more horizontal the black stripe, the more rapid the motion.

In the space-time diagrams displayed in Fig. 3 several successive twists can be recognized. The slopes of the dark stripes are determined from pixels close to the left and right edges of the filament, respectively. The slopes of two successive dark stripes are, with some scatter, almost the same if the brightness of the filament does not change considerably. The mean twist velocity is defined as the mean velocity of two successive twists at the same location in the filament and the error of the velocity measurement is assumed to be the difference between the two such velocity measurements. The mean peak brightness is determined by averaging the maxima of the intensity profiles at several positions along the filament's minor axis between two successive twists. We have repeated this analysis at the inner, middle and outer cut, defined above. The time between two successive twists is found to be approximately 3 to 7 minutes. Within this period the motion of bright penumbral grains along the major axes of the filaments (cf. Sobotka et al. 1999) is small and leads only to negligible errors in the velocity of the twisting motions.

Figure 3 (a to f) shows time slices of filament 'A', at the inner, middle and outer cuts from left to right (i.e. Fig. 3 a, c and e, respectively). Adjacent to each image, the same image is displayed again, but with white lines overplotted on the dark stripes for better visibility. The dependence of the twisting velocity (e.g. the slope of the dark stripes) on the brightness of the body of the filament can be seen. The inner cut, which is the brightest, exhibits the highest velocity. The middle and outer cuts, which are less bright, show lower velocities.

Depicted in Fig. 3g is the time-slice of filament 'B' close to the inner cut in the body of filament at the start of the time series. Figure 3h is the same as 3g, but with white lines overplotted on the dark stripes. With time

this filament penetrates increasingly into the umbra of the spot so that over time the fixed cutting position scans nearly the entire length of the filament. The variation of the twisting velocity with time, and hence with the location in the filament, is well illustrated.

We find a variation of the velocity with location in the filament for nearly each of the 43 studied filaments of this spot. The same behavior is seen, irrespective of a filament's location in the inner, middle or outer penumbra. In general, the filament's intensity decreases over its body, from head to tail, as does the twisting velocity.

Twisting penumbral filaments are also found in the time series of the spots located at $\theta = 38^\circ$ and $\theta = 30^\circ$, respectively. In these time series in total 20 twisting filaments were studied. No significant dependence of the twisting velocities on the viewing angle was found. The only difference to the spot located at $\theta = 48^\circ$ is that in this latter spot the normalized intensities of the filaments are higher.

In Fig. 4 (left) scatter plots of the twisting velocity vs. mean peak intensity at all three locations of the body of the filaments are shown. The upper panel displays the relationship for the 43 filaments of the spot located at $\theta = 48^\circ$, for which a total of 129 data points are plotted (i.e. 3 cuts per filament). The error bars represent the error of each velocity measurement, defined above. The solid line shows a linear fit and the $\pm 1\sigma$ standard deviation of the fit from the data points is indicated by dashed lines. Obviously, the "twisting" motion is stronger in brighter parts of filaments. This is quantified by the linear correlation coefficient, $C = 0.66$, with the probability of a chance correlation lying below 10^{-4} . The lower panel shows the same for all 20 filaments extracted from the analyzed sunspot at $\theta = 38^\circ$ and $\theta = 30^\circ$. For this plot the correlation coefficient is slightly reduced to $C = 0.63$, but the probability of a chance correlation remains below 10^{-4} . In addition, the slopes of the linear regressions in both panels are significant at the 5-10 σ level (see the regression equations given in the upper and lower panels of Fig. 4 (left)). Consequently, both corre-

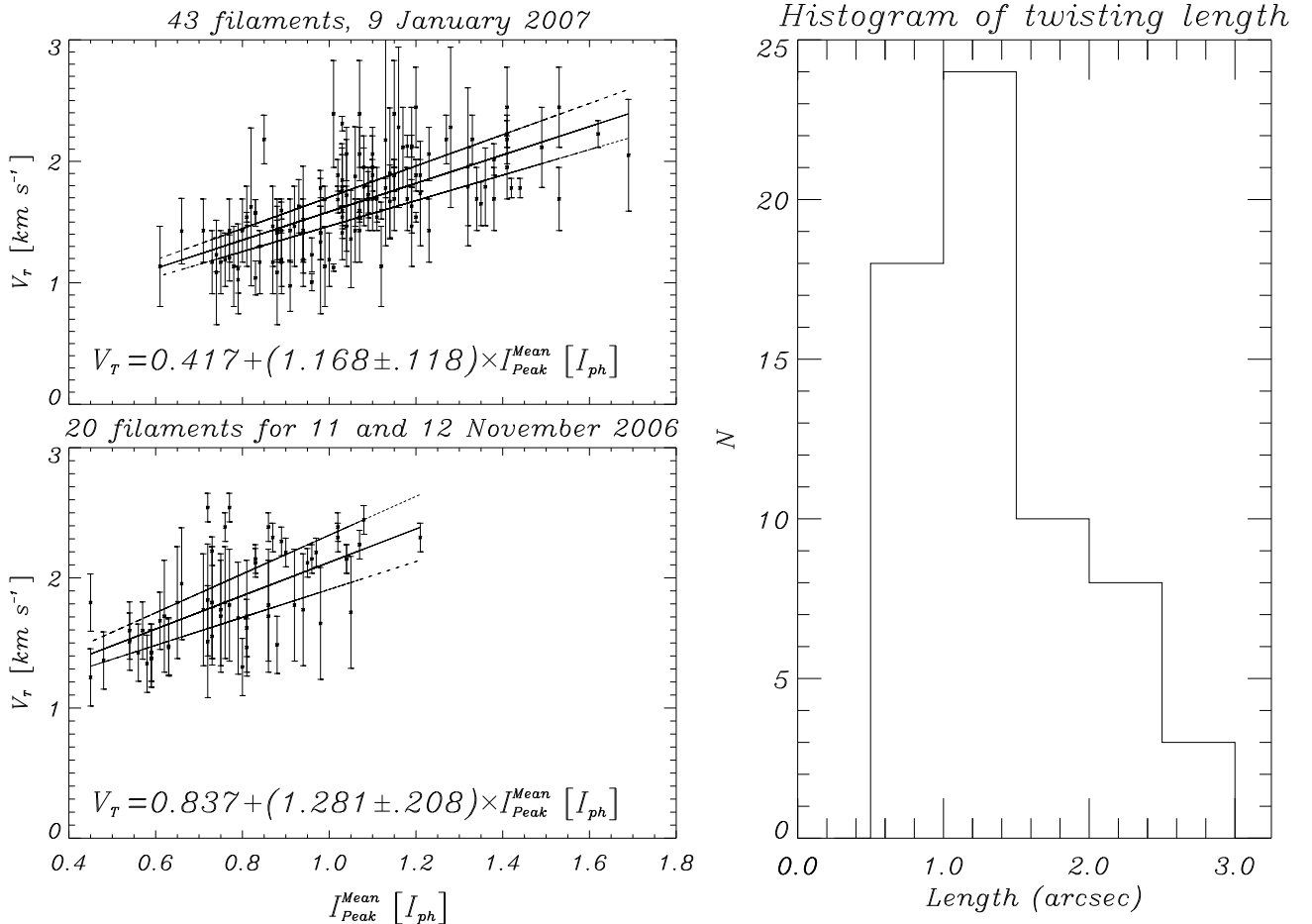


FIG. 4.— Left: Scatter plots for mean peak intensity and twisting velocity for all cuts. Upper panel: scatter plot for 43 twisting filaments observed on 9 January 2007 at $\theta = 48^\circ$. Lower panel: scatter plot for all 20 twisting filaments observed on 11 and 12 November 2006 at $\theta = 38^\circ$ and $\theta = 30^\circ$. The solid lines represent regression fits while the dashed lines indicate $\pm\sigma$ uncertainty in the regression gradient. Right: Histogram of twisting lengths of filaments for all three time series.

lations are statistically significant. The lower normalized intensity of the filaments of the spot located at $\theta = 38^\circ$ and $\theta = 30^\circ$ (lower panel) relative to the spot located at $\theta = 48^\circ$, (upper panel) is evident.

In Fig. 4 (right) a histogram of the twisting length (body) of the filaments from all three time series is depicted. The twisting lengths lie in the range between $0''.5$ and $3''.0$. The mean length of the twisting portion is $1''.4$. In general, the head of the filament, which does not display any twisting motion, has a length about 10% to 20% of the entire filament. However, filaments which extend into the umbra or which are located in the inner penumbra show twists along their entire length, although this is not always clear cut due to the increasing darkening and hence decreasing visibility of stripes in the outer parts of the filaments. In most filaments twists can be seen over fractions of roughly 50% to 70% of their entire length.

Histograms of filament width, mean peak intensity and twisting velocity for inner, middle and outer cuts as obtained from all time series are plotted in Fig. 5. The mean filament widths at the inner, middle and outer cuts are $0''.27 \pm 0.08$, $0''.30 \pm 0.09$ and $0''.28 \pm 0.09$, respectively. Consequently, the widths of the filaments are statistically similar over their twisting length (body of filament). The mean peak intensities are found to be 1.14, 0.97 and 0.79

I_{ph} , respectively, for the three locations. The corresponding mean twisting velocities are 2.11 km s^{-1} , 1.67 km s^{-1} and 1.35 km s^{-1} , respectively.

Scatter plots (not shown here) of width vs. intensity, width vs. velocity and twisting length vs. twisting velocity at inner, middle and outer cuts reveal no significant correlations. However, filaments having larger twisting lengths show lower brightness in middle and outer cuts.

4. DISCUSSION AND CONCLUSION

We analyzed twisting motions at different positions in penumbral filaments viewed from different (heliocentric) angles as observed in time series of seeing-free blue continuum images obtained with *Hinode*. We find that the apparent speed of the twisting motion is related to the local brightness. The parts of the filaments closest to the umbra show the highest brightness and fastest twisting motion. The parts of the filaments further from the umbra are less bright and have lower twist velocities.

These "twisting" motions are most naturally interpreted in terms of overturning convective flows perpendicular to the filament's major axis (Zakharov et al. 2008, Scharmer 2009, Spruit et al. 2010). In particular, Zakharov et al. (2008) have established that such convective motions can transport sufficient energy to explain the brightness of the penumbra. The brightness

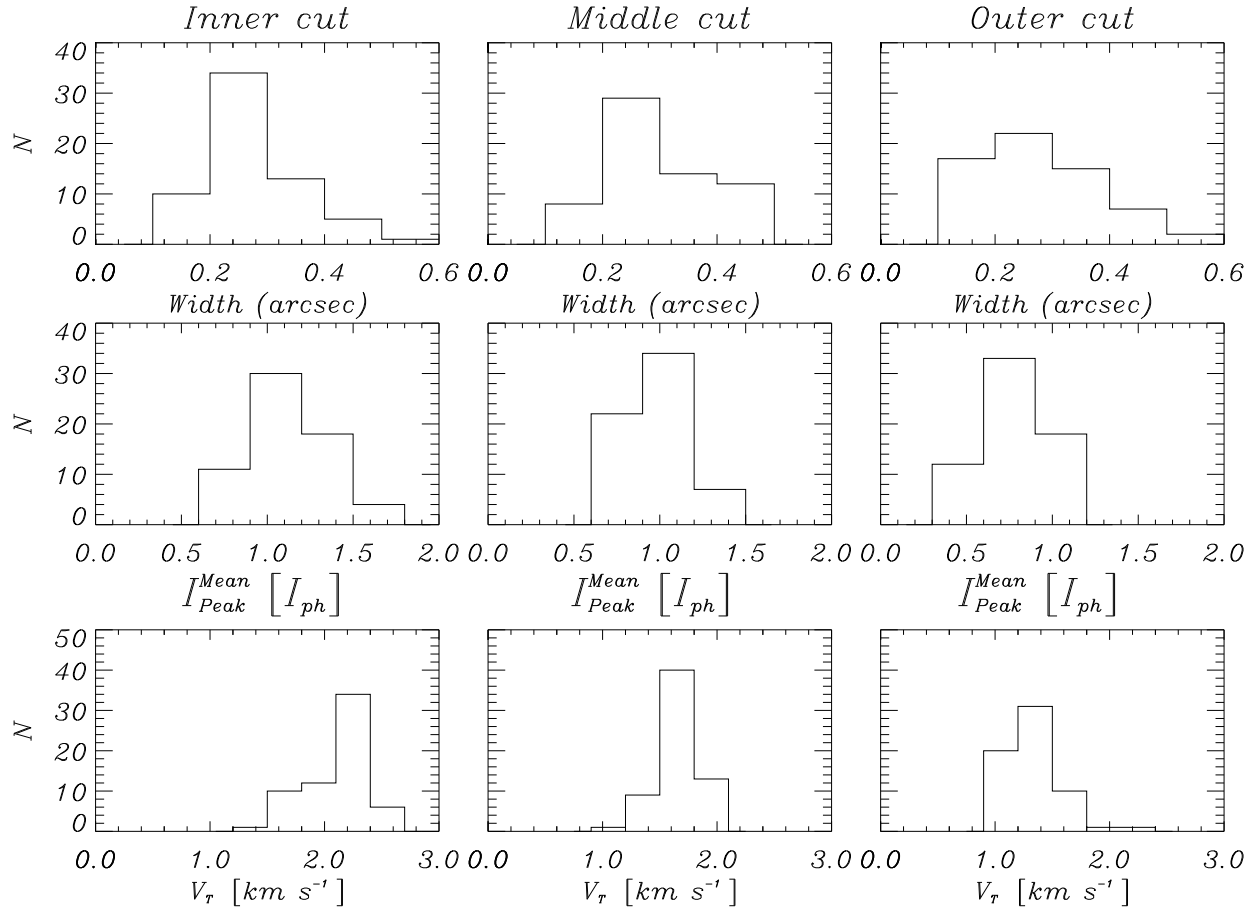


FIG. 5.— Histograms of widths (top panels), normalized mean peak intensities (middle) and twisting velocities (bottom) for inner, middle and outer cuts for all three time series. From left-to-right the histograms for inner, middle and outer cuts are plotted.

variation along the filament's length suggests that such small-scale convection (directed perpendicular to the axis of the filament) is more efficient around the head of the filament and its efficiency decreases gradually towards the filament's tail.

The Evershed effect has been invoked multiple times as a source of heating of the penumbral gas. Schlichenmaier et al. (1998a, b) proposed hot gas to flow into the penumbral photosphere through the cross-section of flux-tubes (cf. Solanki and Montavon 1993). This turns out to be insufficient to heat the penumbra as a whole (Schlichenmaier and Solanki 2003). Scharmer et al. (2008a) and Rempel et al. (2009a, b) have proposed that the Evershed flow in a given filament forms a heavily elongated convective cell which is mainly responsible for keeping the penumbra bright. In this picture, filaments carrying the Evershed flow have a reduced, nearly horizontal magnetic field and gas rises and submerges over large parts of the filament, greatly enhancing the efficiency of convection. Importantly, the gas rising near the axis of symmetry of the filament flows down not just around the tail of a filament, but also at its sides. This component of the flow moving sideways across the filaments is the likely cause of the 'twisting' motions investigated here.

The fact that this clearly convective component of the flow is correlated with the brightness of the filament harboring it significantly strengthens the evidence that

the overturning convection is responsible for heating the penumbra and in particular supports the validity of the energy flux estimate made by Zakharov et al. (2008)¹. Also, it raises the question of the geometry of the flow and of the associated magnetic field in penumbral filaments, which is so far unresolved. Note that observations clearly indicate the presence of a magnetic field in the Evershed flow channels (Solanki et al. 1994) of kG strength (Borrero et al. 2005; Borrero & Solanki 2008, cf. Bellot Rubio et al. 2004, 2007, Jurčák et al. 2007, Scharmer et al. 2008b). Due to the presence of flow components directed along as well as across the axis of the filament, such field lines get twisted.

From the observations alone it is not possible to determine how deep the convective down and upflows reach below the surface. Recently, Spruit et al. (2010) have argued for deep convection. Their criticism of the roll-like convection interpretation is partly based on the misconception that these rolls need to have a circular cross-section. Of course, they can extend much deeper. However, the interpretation of convective rolls does imply that at some point below the surface the surrounding magnetic field wraps around the convective fluid again, separating it from the field-free convecting gas below the

¹ A chance correlation cannot be completely ruled out, however, since rising and sinking of the Evershed flow in the inner and outer penumbra could also produce the observed brightness gradient.

penumbra. This is in contrast to the field-free gap model of Spruit and Scharmer (2006), cf. Scharmer (2009) in which the field-free gap is open at the bottom. Numerical simulations (Heinemann et al. 2008, Rempel et al. 2009) indicate that the convective features reach deep, but are indeed wrapped by the surrounding penumbral field and do not open into the field-free gas surrounding the sunspot. This is the main difference between the two pictures, besides the absence of a magnetic field within the gaps (Spruit and Scharmer 2006), but its presence in the rolls proposed by Zakharov et al. (2008).

The present paper has provided further support for the idea that overturning convection is an important process in maintaining the penumbral temperature. The clear signal of an upflow along the central axis of a bright filament has been reported by Franz & Schlichenmaier (2010) and Ichimoto (2010) but downflows at its sides

has still to be seen, however, although indirect evidence has been found by Márquez et al. (2006) and Sánchez Almeida et al. (2007).

This work has been partly supported by the WCU grant No. R31-10016 funded by the Korean Ministry of Education, Science and Technology. Hinode is a Japanese mission developed and launched by ISAS/JAXA, collaborating with NAOJ as a domestic partner, NASA and STFC (UK) as international partners. Scientific operation of the Hinode mission is conducted by the Hinode science team organized at ISAS/JAXA. Support for the post-launch operation is provided by JAXA and NAOJ (Japan), STFC (U.K.), NASA (U.S.A.), ESA, and NSC (Norway).

REFERENCES

- Bellot Rubio, L. R.; Tsuneta, S.; Ichimoto, K.; Katsukawa, Y. et al., 2007, *ApJ*, 668, L91
 Borrero, J. M.; Lagg, A.; Solanki, S. K.; Collados, M., 2005, *A&A*, 436, 333
 Borrero, J. M.; Solanki, S. K., 2008, *ApJ*, 687, 668
 Evershed, J. 1909, *MNRAS*, 69, 454
 Franz, M.; Schlichenmaier, R.; 2010, *A&A*, 508, 1453,
 Heinemann, T.; Nordlund, .; Scharmer, G. B.; Spruit, H. C.: 2007, *ApJ*, 669, 1390
 Ichimoto, K., Suematsu, Y., Tsuneta, S. et al., 2007, *Science*, 318, 1597
 Ichimoto K., 2010, *ASSP*, "Magnetic Coupling between the Interior and Atmosphere of the Sun", 186
 Jurčák, J.; Bellot Rubio, L.; Ichimoto, K.; Katsukawa, Y. et al., 2007, *PASJ*, 59, 601
 Márquez, I., Sánchez Almeida, J. & Bonet, J. A: 2006, *ApJ*, 638, 553
 Rempel, M., Schüssler, M., Knölker, M. : 2009, *ApJ*, 691, 640
 Rempel, M.; Schüssler, M.; Cameron, R. H.; Knölker, M.: 2009, *Science*, 325, 171
 Sánchez Almeida, J., Márquez, I., Bonet, J. A., & Dominguez Cerdana, I.: 2007, *ApJ*, 658, 1357
 Scharmer, G. B., Nordlund, Å., Heinemann, T. 2008a, *ApJ*, 677, 149
 Scharmer, G. B., 2008b, *Physica Scripta*, 133, 014015
 Scharmer, G. B. 2009, *Space Science Reviews*, 144, 229
 Schlichenmaier, R., Jahn, K., Schmidt, H. U. 1998, *A&A*, 337, 897
 Schlichenmaier, R., Jahn, K., Schmidt, H. U. 1998, *ApJ*, 493, L121
 Schlichenmaier, R., & Solanki, S. K. 2003, *A&A*, 411, 257
 Sobotka, M., Bonet, J. A., & Vázquez, M. 1993, *ApJ*, 415, 832
 Sobotka, M., Brandt, P. N. & Simon, G. W. 1999, *A&A*, 348, 621
 Solanki, S. K.; Montavon, C. A. P.: 1993, *A&A*, 267, 287
 Solanki, S. K.; Schmidt, H. U.: 1993, *A&A*, 267, 287
 Solanki, S. K.; Montavon, C. A. P.; Livingston, W., 1994, *A&A*, 283, 221
 Solanki, S. K.: 2003, *Annu. Rev. Astron. Astrophys.*, 11, 153
 Spruit, H. C.; Scharmer, G. B. and Löfdahl, M. G., 2010, *arXiv:1008.0932v1*
 Spruit, H. C. and Scharmer, G. B.: 2006, *A&A*, 447, 343
 Title, A. M.; Tarbell, T. D.; Topka, K. P.; Ferguson, S. H.; Shine, R. A.; SOUP Team : 1989, *ApJ*, 336, 475
 Tsuneta, S., Ichimoto, K., Katsukawa, Y., et al. 2008, *Sol. Phys.*, 249, 167
 Zakharov, V., Hirzberger, J., Riethmüller, T., Solanki, S.K., & Kobel, P. : 2008, *A&A*, 488, L17